International Journal of Thermophysics, Vol. 23, No. 2, March 2002 (© 2002)

Thermophysical Properties of Chlorine from Speed-of-Sound Measurements

J. J. Hurly[1]

Received May 17, 2001

The speed of sound was measured in gaseous chlorine using a highly precise acoustic resonance technique. The data span the temperature range 260 to 440 K and the pressure range 100 kPa to the lesser of 1500 kPa or 80% of the sample's vapor pressure. A small correction (0.003 to 0.06%) to the observed resonance frequencies was required to account for dispersion caused by the vibrational relaxation of chlorine. The speed-of-sound measurements have a relative standard uncertainty of 0.01%. The data were analyzed to obtain the ideal-gas heat capacity as a function of the temperature with a relative standard uncertainty of 0.1%. The reported values of C_p° are in agreement with those determined from spectroscopic data. The speed-of-sound data were fitted by virial equations of state to obtain the temperature dependent density virial coefficients. Two virial coefficient models were employed, one based on square-well intermolecular potentials and the second based on a hard-core Lennard–Jones intermolecular potential. The resulting virial equations reproduced the sound speed data to within 0.01% and may be used to calculate vapor densities with relative standard uncertainties of 0.1% or less.

KEY WORDS: chlorine; Cl_2; equation of state; intermolecular potential; speed of sound; thermodynamic properties; virial coefficients.

1. INTRODUCTION

Our laboratory has a program to characterize the gases used to manufacture semiconductor devices. Here we report on speed-of-sound measurements $u(T, p)$ in gaseous Cl_2 from 260 to 440 K and pressures up to the lesser of 1.5 MPa or 80% of the vapor pressure. From the $u(T, p)$ data, we

[1] Process Measurements Division, Chemical Science and Technology Laboratory, National Institute of Standards and Technology, Gaithersburg, Maryland 20899. E-mail: john.hurly@nist.gov

0195-928X/02/0300-0455/0 © 2002 Plenum Publishing Corporation

deduce the ideal-gas heat capacity $C_p^o(T)$ and the virial equation of state including both the second $B(T)$ and the third $C(T)$ virial coefficients.

Chlorine is an important industrial chemical, with over 13 million tons produced in 1999 [1]. Chlorine is used in a myriad of applications including disinfecting water for drinking, vinyl plastics chemistry, biochemistry, steel making, and the production of semiconductor devices. Two comprehensive reviews of the properties of chlorine were published during the mid-1980s: *Chlorine International Thermodynamic Tables of the Fluid State—8m Tentative Tables, IUPAC* [2], and *Properties of Chlorine in SI Units*, Chlorine Institute pamphlet 72 [3]. Both reviews correlate the best available experimental data and include properties estimated from models. Reference 2 recommends further measurements to determine the second virial coefficient and the sound speed at low pressures. The present work satisfies these two recommendations.

Figure 1 shows the vapor pressure curve [2], the critical point, and each state point where the speed of sound was measured. These data span most of the region of phase space under the vapor pressure curve. The triple-point temperature of chlorine is approximately 172.17 ± 0.05 K [2]

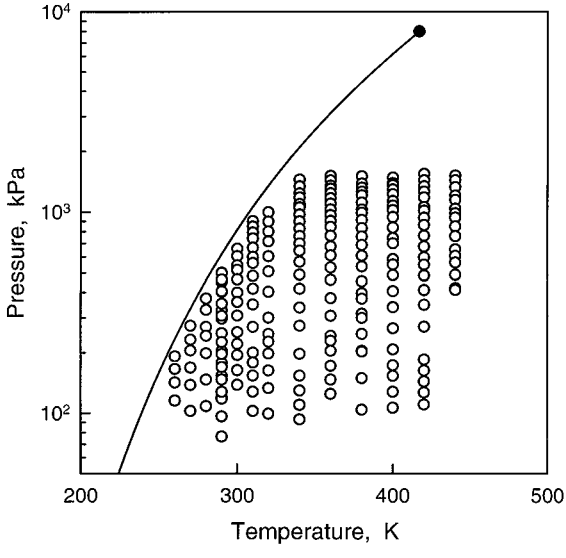

Fig. 1. Phase diagram for Cl_2 with the vapor pressure curve ending at the critical point [2]. The state points at which speed-of-sound measurements were made are shown as open circles.

(IPTS-68), and its critical parameters calculated from the equation of state given in Ref. 2 are reported without uncertainty estimates as $T_c = 416.956$ K, $P_c = 7.9914$ MPa, and $\rho_c = 8.1345\ \text{mol}\cdot\text{dm}^{-3}$. These values lie among the measured values of various authors and are considered as accurate as those reported as measured.

2. EXPERIMENTAL TECHNIQUE AND DATA REDUCTION

The speed of sound is determined with a highly precise acoustic resonance technique. The sample gas is contained in a cylindrical cavity (or resonator) of known dimensions. The acoustic resonance frequencies f of the gas within the cavity are measured as a function of temperature and pressure. Reference [4] provides a description of the current apparatus including the modifications made for handling reactive and hazardous gases. An earlier version of the apparatus was used to study more than 20 nonhazardous gases and gas mixtures [5, 6]. References [7] and [8] describe in detail the acoustic model used to deduce sound speeds from the acoustic resonances within the cylindrical cavity. An additional correction to this acoustic model was required to account for the dispersion associated with the vibrational relaxation of Cl_2. This correction is discussed in Section 3.

At each state point, the frequency of the sound generator was stepped through three resonance modes, and the amplitude and phase of the signal from the detector were recorded. Measurements were made at 11 frequencies spanning $f_{k,n,s} \pm g_{k,n,s}$, where g is the half-width, for each mode (k, n, s). The modes are labeled with the notation (k, n, s) used by Gillis [7]. The theoretically expected function was then fitted to the amplitudes and phases measured at each frequency to obtain both $f_{k,n,s}$ and $g_{k,n,s}$ and a measure of their uncertainties. Typically, the standard deviation of $f_{k,n,s}$ was less than $10^{-5} f_{k,n,s}$. The speed of sound u in the sample gas is determined from the fitted resonance frequencies $f_{k,n,s}$ by $u = 2\pi f_{k,n,s}/k_{k,n,s}$. For our cylindrical cavity with a radius $a = 0.032\ 883$ m and length $l = 0.140\ 468$ m at 273.15 K, the values of the wave number $k_{k,n,s}$ for the modes that we measured, (3,0,0), (4,0,0), and (0,0,1), are 67.0956, 89.4608, and 116.5253 m^{-1}, respectively. The dimensions of the cylinder and their temperature dependence are determined by calibration with argon, a gas for which the speed of sound is accurately know. The measured resonance frequencies were corrected [7, 8] for the thermal and viscous losses at the boundaries using estimates of the transport properties from Ref. 3, a small correction for the fill duct, and an additional correction to account for the dispersion from the vibrational relaxation of chlorine to be discussed later.

3. RELAXATION TIME

Because of the symmetry of the chlorine molecule, tens of thousands ($\approx 40{,}000$ near room temperature) of chlorine–chlorine collisions [9] are required for the vibrational modes of each chlorine molecule to equilibrate with the translational degrees of freedom of chlorine gas. A characteristic time required for these collisions is designated the translation–vibration relaxation time τ, and it varies inversely with the gas density. The effects of the relaxation time are conveniently expressed in terms of C_{vib}, which is the heat capacity of the vibrational modes and in terms of the product $\omega\tau \equiv 2\pi f\tau$, where f is the acoustic frequency. When $\omega\tau \gg 1$, the energy in the vibrational modes is not able to respond to the acoustic wave and the heat capacity of the vibrational modes does not appear in the expression for the speed of sound. When $\omega\tau \sim 1$, part of C_{vib} contributes to the speed of sound and the speed of sound is frequency dependent. When $\omega\tau \ll 1$, nearly all of C_{vib} contributes to the speed of sound.

In this work, $0.003 < \omega\tau < 0.010$. Thus, $\omega\tau \ll 1$ and we used approximate expressions [10] for the increase in resonance frequencies Δf_{rel} and the increase in half-widths Δg_{rel} caused by relaxation:

$$\Delta f_{\text{rel}}/f = 1/2(\gamma-1)(\omega\tau)^2\,\Delta[1-1/4\Delta(3+\gamma)] \tag{1}$$

$$\Delta g_{\text{rel}}/f = 1/2(\gamma-1)(\omega\tau)\,\Delta \tag{2}$$

where $\Delta \equiv C_{\text{vib}}/C_{\text{p}}$. As discussed below, we used an iterative analysis at each temperature. We estimated Δ and used Eq. (2) with experimental values of $\Delta g_{\text{rel}}/f$ to determine τ. Then the observed resonance frequencies $f_{k,n,s}$ were corrected using Eq. (1) and improved values of Δ were obtained.

The acoustic model [7, 8] mentioned in Section 2 was used to predict resonance peak half-widths $g_{k,n,s}$. Experience with other gases in this resonator, e.g., argon, sulfur hexafluoride, and trimethylgallium, shows that the measured half-widths divided by the frequency $g_{k,n,s}/f_{k,n,s}$ are (50 to 150) ppm (1 ppm = 1 part in 10^6) greater than those predicted by the model. This is referred to as the excess half-width. The magnitude of the excess half-widths was independent of the gas being studied, so it is assumed not to be a function of the gas properties, but a consistent artifact of the experimental apparatus. These "normal" excess half-widths do not affect the measured resonance frequencies within the stated uncertainties. The excess half-widths are attributed to gaps in the sealing surfaces, the acoustic transducers, surface roughness, and other uncharacterized experimental irregularities. For the chlorine measurements, excess half-widths were often greater than 300 ppm of $f_{k,n,s}$. These increased losses were caused by the vibrational relaxation of chlorine.

We assumed that the vibrational relaxation time τ was inversely proportional to the density ρ and that the intramolecular energy exchange between vibrational modes is rapid enough that the vibrational contribution to the heat capacity can be described with a single relaxation time. We subtracted the thermal, viscous, and the fill duct contributions from the observed half-widths as prescribed for each mode by the acoustic model, along with a "normal" 100 ppm excess half-width seen independent of the gas being studied. The remainder was ascribed to the vibrational relaxation, Δg_{rel}. Using Eq. (2), a value for τ was determined for each measured half-width at each temperature–pressure state point. The equation of state and heat capacities were taken from Ref. 3. The values of τ ranged from 0.8 to 5 μs. The values of the product $\tau\rho$ were fitted by an empirical function of the temperature,

$$\tau\rho = (0.06326\ \mu\text{s}\cdot\text{kg}\cdot\text{m}^{-3})\exp(1128.87\ \text{K}/T) \tag{3}$$

Figure 2 shows this function along with the value of $\tau\rho$ obtained for each resonance. The spread among the three measured modes provides a

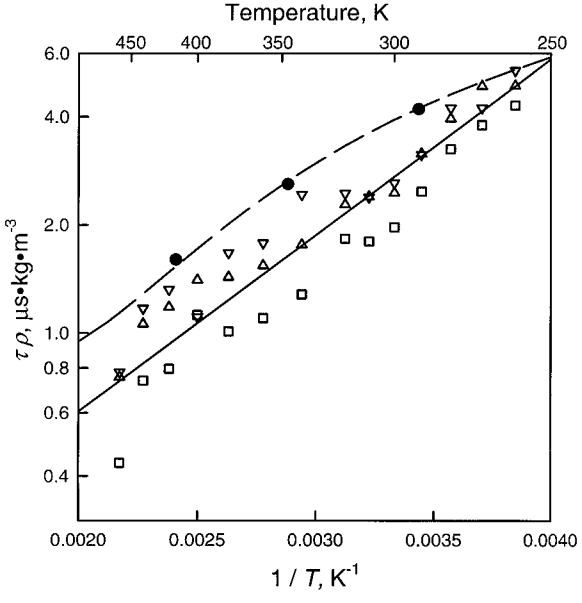

Fig. 2. The product of the relaxation time τ and the density ρ as a function of inverse temperature. The symbols identify the resonance modes: △ (3,0,0), ▽ (4,0,0), and □ (1,0,0). The solid line is the fit to the present acoustic results, Eq. (2). The published values of Eucken and Becker [30] are shown as ●, and the dashed curve is a fit to their values including points outside the shown temperature range.

Table I. Speed of Sound in Chlorine

p (kPa)	u (m·s^{-1})	$10^6 \frac{\sigma[u]}{u}$
	$T = 260.00$ K	
191.73	197.372	6
165.90	197.982	53
142.01	198.544	93
115.51	199.149	91
	$T = 270.00$ K	
273.13	199.676	57
232.91	200.555	61
205.31	201.143	41
168.48	201.920	78
138.04	202.543	19
102.60	203.272	88
	$T = 280.00$ K	
373.34	201.804	45
328.22	202.714	68
269.83	203.876	44
243.40	204.385	53
198.69	205.241	50
146.79	206.226	115
108.40	206.928	78
108.40	206.923	66
	$T = 290.01$ K	
500.92	203.619	67
450.12	204.588	66
402.94	205.461	35
325.71	206.866	54
296.53	207.386	65
250.73	208.188	74
204.15	208.983	40
177.90	209.434	37
153.33	209.852	29
127.97	210.280	86
119.67	210.409	144
118.05	210.440	122
	$T = 290.01$ K	
499.41	203.644	66
463.09	204.335	53
405.50	205.414	89

Table I. *(Continued)*

p (kPa)	u (m·s^{-1})	$10^6 \frac{\sigma[u]}{u}$
351.75	206.394	53
306.17	207.209	50
226.39	208.606	48
196.82	209.106	106
169.78	209.576	110
146.99	209.970	112
127.61	210.295	108
96.43	210.809	39
76.50	211.128	0
	$T = 300.00$ K	
658.82	205.116	111
605.55	206.067	87
545.19	207.127	81
516.79	207.618	80
464.36	208.512	79
399.66	209.596	81
359.17	210.260	75
307.38	211.098	81
253.92	211.948	86
221.70	212.456	89
194.69	212.884	113
163.56	213.361	79
138.32	213.747	8
	$T = 310.00$ K	
901.89	205.415	28
847.96	206.351	63
792.34	207.298	52
740.54	208.167	55
666.69	209.377	50
599.67	210.451	59
559.27	211.087	54
483.30	212.260	60
417.79	213.256	57
348.85	214.284	57
269.77	215.438	50
200.23	216.433	74
178.65	216.745	88
153.87	217.088	30
127.92	217.450	75
102.58	217.808	79

Table I. *(Continued)*

p (kPa)	u (m·s^{-1})	$10^6 \frac{\sigma[u]}{u}$
	$T = 320.00$ K	
998.78	208.547	119
896.62	210.171	95
801.77	211.609	104
716.37	212.898	85
604.46	214.510	113
508.31	215.880	73
403.65	217.309	103
299.88	218.711	94
248.63	219.390	76
227.66	219.668	90
198.22	220.053	102
163.04	220.512	118
133.25	220.890	69
99.55	221.313	47
	$T = 340.00$ K	
1447.60	211.433	78
1342.19	212.934	136
1237.52	214.378	112
1181.70	215.125	152
1095.54	216.259	129
1054.54	216.794	96
972.87	217.832	91
899.35	218.758	83
828.80	219.627	121
761.21	220.462	87
700.37	221.189	113
643.53	221.876	85
567.63	222.772	75
489.55	223.668	76
417.57	224.510	74
337.04	225.423	78
273.29	226.139	77
197.53	226.982	115
153.72	227.460	140
129.75	227.707	70
110.02	227.902	108
110.02	227.908	272
93.16	228.098	260

Table I. *(Continued)*

p (kPa)	u (m·s^{-1})	$10^6 \frac{\sigma[u]}{u}$
	$T = 360.00$ K	
1511.92	220.055	175
1436.77	220.909	190
1352.12	221.862	221
1305.92	222.381	199
1238.91	223.106	228
1171.05	223.845	146
1101.31	224.596	129
1030.62	225.346	114
966.40	226.020	113
904.61	226.662	102
845.51	227.270	105
763.27	228.110	103
676.15	228.991	100
609.83	229.659	85
531.65	230.430	88
462.03	231.113	80
374.94	231.958	68
306.72	232.607	108
243.69	233.204	102
230.01	233.338	98
204.88	233.576	100
172.19	233.888	85
146.96	234.143	168
124.83	234.332	158
	$T = 380.00$ K	
1504.09	228.757	164
1382.99	229.873	255
1321.50	230.437	183
1261.63	230.987	198
1211.67	231.440	199
1114.89	232.306	198
1029.69	233.073	110
991.71	233.405	175
914.29	234.089	89
833.14	234.793	97
756.90	235.447	92
687.63	236.037	90
608.14	236.711	91

Table I. *(Continued)*

p (kPa)	u (m·s^{-1})	$10^6 \frac{\sigma[u]}{u}$
537.61	237.304	93
454.12	237.998	100
396.60	238.474	104
372.88	238.670	97
313.96	239.155	96
299.34	239.275	95
248.79	239.684	92
205.09	240.044	101
202.91	240.067	106
149.47	240.502	66
104.19	240.858	48
	$T = 400.00$ K	
1484.50	236.872	176
1484.26	236.875	171
1483.98	236.872	187
1483.81	236.877	171
1483.61	236.881	182
1483.45	236.881	175
1392.79	237.583	154
1359.30	237.839	311
1295.92	238.334	206
1226.63	238.850	152
1135.39	239.534	187
1077.71	239.979	136
1022.73	240.392	134
944.98	240.972	121
838.80	241.756	116
743.97	242.451	106
700.74	242.766	103
584.81	243.606	95
550.52	243.853	91
487.70	244.304	88
406.53	244.885	88
338.87	245.364	83
265.62	245.880	57
208.09	246.288	90
173.40	246.525	83
153.52	246.660	39
127.92	246.836	18
106.64	246.982	110

Table I. *(Continued)*

p (kPa)	u (m·s^{-1})	$10^6 \frac{\sigma[u]}{u}$
	$T = 420.00$ K	
1546.06	243.926	170
1439.12	244.616	181
1344.50	245.230	264
1262.65	245.760	210
1183.15	246.272	174
1060.42	247.059	145
1018.01	247.331	145
938.16	247.839	133
863.59	248.310	142
764.76	248.935	127
676.29	249.494	104
597.36	249.983	107
549.40	250.281	127
485.37	250.680	110
411.60	251.137	122
348.23	251.524	105
270.70	251.996	89
185.26	252.520	48
163.23	252.653	78
144.00	252.761	94
127.01	252.859	81
110.58	252.948	73
	$T = 440.00$ K	
1516.76	251.197	131
1440.55	251.628	160
1328.48	252.239	148
1206.97	252.919	111
1149.56	253.229	130
1039.81	253.829	133
988.26	254.114	118
939.72	254.374	116
849.97	254.859	129
760.28	255.352	101
653.82	255.924	102
606.76	256.174	74
562.89	256.405	70
490.02	256.793	90
421.30	257.171	77
412.51	257.218	72

measure of the uncertainty in the relaxation time given in Eq. (3). Also included in Fig. 2 are three values of relaxation times in chlorine obtained from shock-tube measurements [11]. The near-agreement of the two data sets is acceptable, considering the different conditions found in shock-tube experiments.

The measured frequencies were corrected for relaxation by using Eq. (1) and the values of τ from Eq. (3) and gas properties from Ref. 3. A single iteration was performed which demonstrated convergence of the calculation. The reported values of the speed of sound were determined from the corrected frequencies. Trusler et al. applied similar corrections for vibrational relaxation in carbon monoxide [12], methane [13], and nitrogen [14, 15].

4. RESULTS

A total of 222 speed-of-sound measurements is tabulated along 13 isotherms between 260 and 440 K and pressures up to 1.5 MPa or 80% of the vapor pressure. At each temperature and pressure, one radial and two longitudinal modes were used to compute the tabulated values of the speed of sound. The weighted mean of these three values and their relative standard deviation $\sigma[u]/u \times 10^6$ with coverage factor of $k=1$ are listed in Table I.

5. ACOUSTIC EQUATION OF STATE

Figure 3 (top) shows the speed-of-sound measurements along individual isotherms. The data on each isotherm were fitted by the acoustic virial equation of state, given as

$$u^2 = \frac{\gamma^0 RT}{m}\left(1 + \frac{\beta_a p}{RT} + \frac{\gamma_a p^2}{RT} + \frac{\delta_a p^3}{RT} + \cdots\right) \tag{4}$$

where m is molar mass, R is the universal gas constant, T is the temperature in kelvins (ITS-90), C_p° and C_v° are the constant-pressure and constant-volume ideal-gas heat capacities, $\gamma^0 = C_p^\circ/C_v^\circ$ is the zero-pressure limit of the heat-capacity ratio, and β_a, γ_a, and δ_a are the temperature-dependent acoustic virial coefficients. Only the first two acoustic virial coefficients were required for the gas densities spanned by our measurements. On each isotherm, C_p° is obtained from the zero-pressure intercept of Eq. (4) through the relation $C_p^\circ/R = \gamma^0/(\gamma^0 - 1)$. The resulting values of C_p°/R are listed in Table II together with values of β_a and γ_a. The two lowest temperature isotherms have a small pressure range because of the low vapor pressure. Consequently, they have larger uncertainties for C_p°.

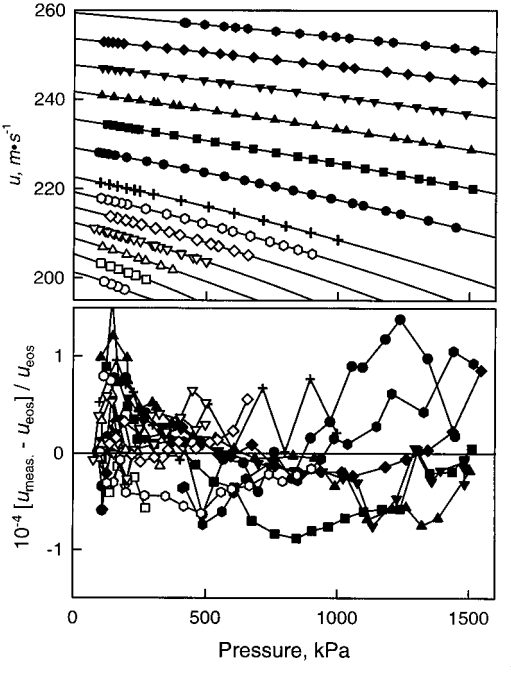

Fig. 3. Top: Sound speed in Cl_2 vs pressure for various isotherms and individual fits to Eq. (4). Bottom: Deviations from the HCSW equation of state. This bottom figure is also representative of the deviation plot for the HCLJ equation of state. (○) 260 K; (□) 270 K; (△) 280 K; (▽) 290 K; (◇) 300 K; (⬡) 310 K; (+) 320 K; (●) 340 K; (■) 360 K; (▲) 380 K; (▼) 400 K; (◆) 420 K; (⬢) 440 K.

Chlorine is a simple diatomic with a single vibrational mode. This allows accurate calculation of the ideal-gas heat capacity from statistical mechanics and spectroscopy. Over our experimental temperature range spanning 260 to 440 K, the value of C_p° obtained from three independent estimations differ by at most 0.042% (see Fig. 4). Within this uncertainty, we can consider the difference between these estimates and our determinations of C_p° for Cl_2 to be a measure of the uncertainties from our experimental techniques and the acoustic model.

The C_p° values for Cl_2 reported in Table II were fitted with Eq. (5), the expression for the ideal-gas heat capacity for a harmonic oscillator:

$$\frac{C_p^\circ}{R} = \frac{C_{p,t}^\circ + C_{p,r}^\circ}{R} + \frac{(\Theta_{vib}/T)^2 \exp(\Theta_{vib}/T)}{(\exp(\Theta_{vib}/T) - 1)^2} \tag{5}$$

Table II. Properties from Individual Fits of the Isotherms to Eq. (4)

T (K)	$C_p^o(T)$ (R)	$\beta_a(T)$ ($cm^3 \cdot mol^{-1}$)	$\gamma_a(T)$ ($cm^3 \cdot mol^{-1} \cdot MPa^{-1}$)
260	3.993±0.034	−453.2±38	−126±120
270	4.017±0.021	−425.0±18	−76±140
280	4.043±0.006	−390.0±5.2	−66±10
290	4.069±0.002	−357.6±2.3	−59±3.5
290	4.066±0.005	−361.5±3.7	−54±5.8
300	4.088±0.002	−336.0±2.0	−45±2.5
310	4.111±0.002	−312.4±0.7	−39±0.7
320	4.127±0.002	−293.4±1.3	−31±1.1
340	4.163±0.002	−258.1±0.8	−21±0.5
360	4.190±0.002	−231.9±0.8	−12±0.5
380	4.218±0.002	−206.6±0.8	−8.1±0.5
400	4.244±0.002	−184.5±0.8	−5.0±0.5
420	4.267±0.002	−165.5±0.9	−2.8±0.5
440	4.289±0.002	−147.9±1.7	−1.4±0.6

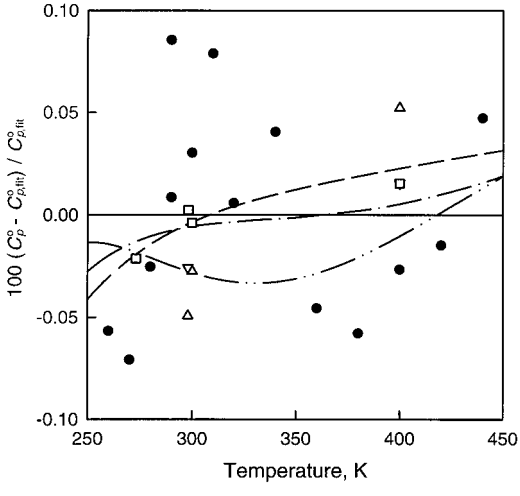

Fig. 4. Percentage deviations of ideal-gas heat capacity calculated from Eq. (5); (●) present work. Also shown are values predicted from spectroscopic data and commonly used polynomial fits to these values: (- - -) [31]; (-···) [2]; (-·-·) [3]; (□) [32]; (△) [33]; (△) [34].

Equation (5) assumes that (1) the electronic contributions to the heat capacity are negligible, (2) the translational $C^{\circ}_{p,t}$ and rotational $C^{\circ}_{p,r}$ contributions are independent of temperature, and (3) the vibrational contribution has the Einstein form. The fit yielded $C^{\circ}_{p,t} + C^{\circ}_{p,r} = (3.534 \pm 0.012)\, R$ and the characteristic vibrational temperature $\Theta_{vib} = 822.9 \pm 18.0$ K. The relative standard deviation of the fit was 0.042%. Figure 4 shows the deviations of the measured values of C°_{p} from Eq. (5), as well as other reported values calculated from spectroscopy. Equation (5) does not consider anharmonicity, which probably explains why the fitted value of $C^{\circ}_{p,t} + C^{\circ}_{p,r}$ differs from the value of $3.5R$ expected for a harmonic oscillator. The spectroscopically determined values of Θ_{vib} of 797.3 [16], 810 [17], and 803.3 K [18] all agree reasonably well with the fitted value.

6. THE DENSITY VIRIAL EQUATION OF STATE

A density equation of state $\rho(T, p)$ for the gas phase was obtained by fitting the entire $u^2(T, p)$ surface. The virial equation of state,

$$p = RT\rho[1 + B(T)\,\rho + C(T)\,\rho^2 + \cdots] \tag{6}$$

is the appropriate choice for the gas phase. Here p is pressure, and $B(T)$ and $C(T)$ are the second and third density virial coefficients. The acoustic virial coefficients in Eq. (4) are directly related to the density virial coefficients in Eq. (6) through exact thermodynamic relations involving the density virial coefficients, their temperature derivatives, and $\gamma^0(T)$ [19]. Equation (6) was fitted directly to the $u^2(T, p)$ surface using these relationships together with a model for the temperature dependence of the density virial coefficients, and $\gamma^0(T)$ computed from Eq. (5).

A simple spherically symmetric potential model is satisfactory for the accurate fitting of virial coefficients to speed-of-sound measurements [20]. This is because the average over all collision orientations is approximated by a spherical model. Two models for the density virial coefficients and their temperature dependence were considered: (1) the hard-core square-well (HCSW) model and (2) the hard-core Lennard–Jones (HCLJ) model. The implementation of both of these models was described in detail elsewhere [4, 21–23]; here only the results are provided.

6.1. The Hard-Core Square-Well Potential Model (HCSW)

The HCSW model of molecular interactions is an algebraically simple representation of intermolecular interactions that has explicit algebraic expressions for the temperature-dependent second and third virial coefficients [19] $B(T)$ and $C(T)$. These expressions are

$$B(T) = b_o[1-(\lambda^3-1)\,\Delta]$$
$$C(T) = \tfrac{1}{8} b_o^2(5-c_1\Delta-c_2\Delta^2-c_3\Delta^3) \quad (7)$$

$$c_1 = \lambda^6-18\lambda^4+32\lambda^3-15$$
$$c_2 = 2\lambda^6-36\lambda^4+32\lambda^3+18\lambda^2-16 \quad (8)$$
$$c_3 = 6\lambda^6-18\lambda^4+18\lambda^2-6$$

where $\Delta = \exp[\varepsilon/(k_B T)-1]$ and k_B is Boltzmann's constant. The adjustable parameters are: ε the well depth, σ the hard-core diameter, and λ the ratio of the width of the well to σ. Here, b_o is the molar volume of the hard core $b_o = 2/3\pi N_A \sigma^3$, and N_A is Avogadro's constant. Equations (7) and (8) allow the $u^2(T, p)$ surface to be fitted directly to Eq. (6). We followed Ref. 19 in using different values of b_o, ε, and λ for $B(T)$ and $C(T)$; thus, this model has six parameters. We used the functional forms of Eqs. (7) and (8), for their physical temperature dependences; we do not attribute physical significance to the fitted parameters.

To fit the data, the ideal-gas heat-capacity was fixed at the values given by Eq. (5) and the six parameters, b_o, ε, and λ for $B(T)$ and b_o, ε, and λ for $C(T)$, were allowed to vary. The resulting parameters are listed in Table III. All of our reported sound speeds are fitted to within $\pm 0.01\%$. The fit had 216 degrees of freedom v, and χ^2/v was 0.30, where $\chi^2 = \sum_i [f(x_i)-f_i]^2/\sigma_f^2$; and $f(x_i) = u^2(T, p)$. Figure 3 (bottom) shows the deviation plot of the measured speeds of sound from the HCSW equation of state.

6.2. Hard-Core Lennard–Jones (HCLJ) Model

The HCLJ analysis is similar to the HCSW analysis; however, multiple numerical integrations are required at each temperature to determine the virial coefficients and their temperature derivatives. We used the hard-core Lennard–Jones 6–12 potential [24] given by

$$\varphi(r) = 4\varepsilon\left\{\left(\frac{\sigma-2a}{r-2a}\right)^{12}-\left(\frac{\sigma-2a}{r-2a}\right)^{6}\right\} \quad (9)$$

Table III. Parameters for HCSW Equation of State for Chlorine

	b_o ($m^3 \cdot mol^{-1}$)	λ	ε/k_B (K)
$B(T)$ ($m^3 \cdot mol^{-1}$)	5.51828×10^{-5}	1.52270	370.89
$C(T)$ ($m^3 \cdot mol^{-1}$)^2	8.07257×10^{-5}	1.43755	347.86

where r is the intermolecular separation, ε is the well depth, σ is the value of r where $\varphi(r)$ crosses zero, and a is the radius of the hard core. This potential has three adjustable parameters: ε, σ, and a. We calculated the classical second and third virial coefficients and their temperature derivatives [25, 26] using an automatic adaptive quadrature routine [27], where one can specify the desired accuracy, which we set to 10^{-4}. The calculation of the third virial coefficient using only the pairwise-additive contribution underestimates the third virial coefficient. It is required to include a non-pairwise-additive three-body contribution to the potential. Following Trusler [29], we used the Axilrod–Teller triple–dipole term [28], adding a fourth adjustable parameter, v_{123}, the leading three-body dispersion coefficient. The integral equations providing the second and third virial coefficients for spherically symmetric molecules are given in Ref. 29.

With $C_p^o(T)$ given by Eq. (5), only four potential parameters, ε, σ, a, and v_{123} are required to fit the $u^2(T, p)$ data. The resulting parameters are given in Table IV. As in the case of the HCSW model, all sound-speed measurements are fitted within $\pm 0.01\%$. The fit had 218 degrees of freedom v, and χ^2/v was 0.29. The deviations of the measured sound speeds from those calculated from the deduced HCLJ equation of state are essentially the same as the deviations from the HCSW (Fig. 3, bottom).

The computation of the second and third virial coefficients and their temperature derivatives using the four potential parameters is a numerically intensive process and is not convenient for repetitive calculations. Again, following the lead of Trusler [29], we provide a lookup table for the second and third virial coefficients and their first two temperature derivatives to allow interpolation. In the lookup table, a substitution of variables has been performed. The temperature is replaced by a reduced reciprocal temperature $\tau = \varepsilon/k_B T$, where $T(dB/dT) = -\tau(dB/d\tau)$ and $T^2(d^2B/dT^2) = \tau^2(d^2B/d\tau^2) + 2\tau(dB/d\tau)$. Table V provides the virial coefficients in reduced (unitless) form where $B^*(T) = B(T)/b_0$ and $C^*(T) = C(T)/b_0^2$, where $b_0 = 2/3\pi N_A \sigma^3$. Table V list these calculated values and spans the reduced temperature range $0.3 \leqslant \tau \leqslant 3.0$, which corresponds to 177 to 1770 K. This range greatly exceeds our experimental temperature range; however, the extrapolated virial coefficients are reliable and expected to

Table IV. Hard-Core Lennard–Jones Potential Parameters

	σ (nm)	ε/k_B (K)	a (nm)	v_{123}/k_B (K·nm^9)
Cl_2	0.380 817	531.02	0.049 977	0.007 560 412

Table V. Reduced Virial Coefficients and Derivatives with Respect to the Inverse Reduced Temperature Calculated from the HCLJ Model

τ	$B(\tau)^*$	$\frac{\partial B(\tau)^*}{\partial \tau}$	$\frac{\partial^2 B(\tau)^*}{\partial \tau^2}$	$\frac{\partial^3 B(\tau)^*}{\partial \tau^3}$	$C(\tau)^*$	$\frac{\partial C(\tau)^*}{\partial \tau}$	$\frac{\partial^2 C(\tau)^*}{\partial \tau^2}$	$\frac{\partial^3 C(\tau)^*}{\partial \tau^3}$
0.3	0.03439	−0.17055	−0.19457	0.59314	0.00377	0.00109	0.01161	0.09626
0.4	0.01644	−0.18792	−0.15918	0.19046	0.00395	0.00262	0.01820	0.04353
0.5	−0.00312	−0.20318	−0.14846	0.04483	0.00430	0.00461	0.02114	0.01702
0.6	−0.02418	−0.21793	−0.14773	−0.02298	0.00487	0.00677	0.02178	−0.00408
0.7	−0.04672	−0.23289	−0.15210	−0.06145	0.00566	0.00889	0.02026	−0.02683
0.8	−0.07078	−0.24846	−0.15961	−0.08731	0.00664	0.01074	0.01623	−0.05509
0.9	−0.09644	−0.26489	−0.16938	−0.10739	0.00779	0.01203	0.00895	−0.09209
1.0	−0.12379	−0.28239	−0.18100	−0.12483	0.00902	0.01239	−0.00260	−0.14129
1.1	−0.15296	−0.30115	−0.19431	−0.14127	0.01022	0.01132	−0.01985	−0.20688
1.2	−0.18407	−0.32131	−0.20925	−0.15761	0.01121	0.00817	−0.04470	−0.29416
1.3	−0.21727	−0.34305	−0.22585	−0.17444	0.01175	0.00205	−0.07963	−0.40988
1.4	−0.25274	−0.36654	−0.24417	−0.19215	0.01148	−0.00820	−0.12791	−0.56275
1.5	−0.29064	−0.39195	−0.26432	−0.21103	0.00992	−0.02412	−0.19379	−0.76404
1.6	−0.33120	−0.41947	−0.28643	−0.23136	0.00641	−0.04773	−0.28281	−1.02829
1.7	−0.37461	−0.44930	−0.31065	−0.25336	0.00003	−0.08169	−0.40217	−1.37432
1.8	−0.42114	−0.48167	−0.33716	−0.27726	−0.01039	−0.12948	−0.56120	−1.82647
1.9	−0.47104	−0.51682	−0.36617	−0.30328	−0.02647	−0.19565	−0.77203	−2.41618
2.0	−0.52461	−0.55500	−0.39790	−0.33167	−0.05033	−0.28613	−1.05037	−3.18413
2.1	−0.58215	−0.59650	−0.43259	−0.36267	−0.08477	−0.40865	−1.41654	−4.18293
2.2	−0.64403	−0.64162	−0.47053	−0.39656	−0.13346	−0.57324	−1.89689	−5.48058
2.3	−0.71061	−0.69072	−0.51201	−0.43362	−0.20125	−0.79296	−2.52552	−7.16504
2.4	−0.78231	−0.74415	−0.55737	−0.47418	−0.29445	−1.08474	−3.34655	−9.35011
2.5	−0.85960	−0.80233	−0.60697	−0.51858	−0.42132	−1.47057	−4.41709	−12.18299
2.6	−0.94295	−0.86570	−0.66122	−0.56721	−0.59264	−1.97892	−5.81103	−15.85418
2.7	−1.03293	−0.93475	−0.72057	−0.62047	−0.82241	−2.64671	−7.62401	−20.61027
2.8	−1.13011	−1.01000	−0.78549	−0.67881	−1.12887	−3.52177	−9.97979	−26.77056
2.9	−1.23515	−1.09205	−0.85652	−0.74275	−1.53572	−4.66605	−13.03857	−34.74860
3.0	−1.34877	−1.18153	−0.93424	−0.81283	−2.07370	−6.15976	−17.00778	−45.08024

predict gas densities over this extended temperature range to within 0.1% [19] as demonstrated by our experience with CF_4 and C_2F_6 [4] and SF_6 [22] and the experience of Trusler et al. with C_3H_8 [29].

7. DISCUSSION

Speed-of-sound measurements in the vapor phase of chlorine at 222 state points along 13 isotherms between 260 and 440 K and pressures up to 1.5 MPa or 80% of the vapor pressure have been reported. The ideal-gas heat capacity was determined from each isotherm by fitting the acoustic virial equation Eq. (4). The measured values of C_p^o agree with those calculated from spectroscopy to within 0.1%. The second and third virial coefficients were determined by fitting the density virial equation of state Eq. (6) to the experimental speed-of-sound surface. This was done with two models for the virial coefficients, the HCSW and the HCLJ. Figure 5

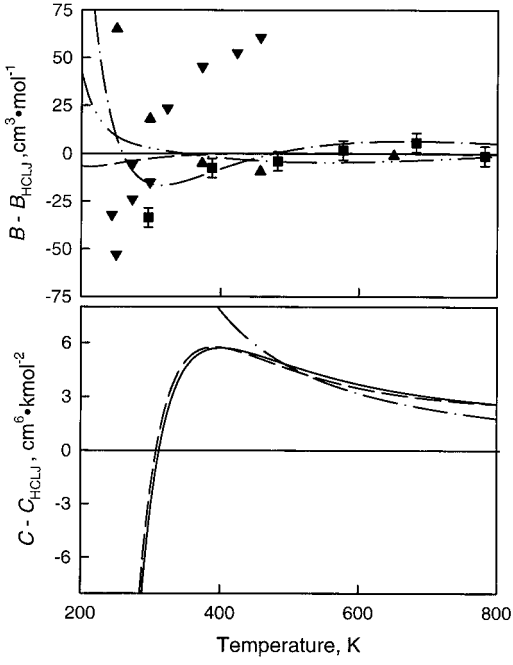

Fig. 5. The top figure shows the deviations of the second virial coefficient from those calculated from the HCLJ model. The bottom figure shows the third virial coefficients. (—) HCLJ; (- - -) HCSW; (- · · -) [3]; (- · · ·) [2]; (■) [35]; (▲) [36]; (▼) [37].

compares the resulting values of $B(T)$ and $C(T)$ with previously published values and those extracted from the equations of state given in Refs. 2 and 3. No previous measurements of the third virial coefficient are available for comparison. The virial equation of state presented here is the most accurate description of the vapor phase of chorine, and should be used for vapor phase calculations of $\rho(T, p)$.

The IUPAC volume [2] and Chlorine Institute Pamphlet 22 [3] contain two widely used global equations of state. The measured speeds of sound differ from those determined by the equation of state from Ref. 3 by only $\pm 0.2\%$. The equation of state in Ref. 2 predicts speeds of sound with a positive bias up to $+0.5\%$. Both equations of state predict gas densities to better than 0.1% at pressures below 1.0 MPa or 80% the vapor pressure. Once these results, along with other experimental work recommended by Ref. 2 become available, the IUPAC tentative thermodynamic tables of the fluid state for chorine can be revised and will no longer have to be considered tentative.

ACKNOWLEDGMENT

This work was supported in part by the National Semiconductor Metrology Program.

REFERENCES

1. Facts & figures for the chemical industry, *Chem Eng. News* **78**:45 (2000).
2. S. Angus, B. Armstrong, and K. M. de Reuck, *Chlorine, International Thermodynamic Tables of the Fluid State—8m Tentative Tables, IUPAC* (Pergamon Press, Oxford, 1985).
3. Chlorine Institute, *Properties of Chlorine in SI Units*, 2nd ed. (Chlorine Institute, Washington, DC, 1986).
4. J. J. Hurly, *Int. J. Thermophys.* **20**:455 (1999).
5. A. R. H. Goodwin and M. R. Moldover, *J. Chem. Phys.* **95**:5236 (1991).
6. K. A. Gillis, *Int. J. Thermophys.***18**:73 (1997).
7. K. A. Gillis, *Int. J. Thermophys.***15**:821 (1994).
8. K. A. Gillis, A. R. H. Goodwin, and M. R. Moldover, *Rev. Sci. Instrum.* **62**:2213 (1991).
9. A. Eucken and R. Becker, *Z. Phys. Chem.* **B27**:235 (1935).
10. J. P. M. Trusler, *Physical Acoustics and Metrology of Fluids* (Adam Hilger, Bristol, UK, 1991).
11. E. F. Smiley and E. H. Winkler, *J. Chem. Phys.* **22**:2018 (1954).
12. A. F. Estrada-Alexanders and J. P. M. Trusler, *J. Chem. Thermodyn.* **30**:1589 (1998).
13. J. P. M. Trusler and M. Zarari, *J. Chem. Thermodyn.* **24**:973 (1992).
14. M. F. Costa Gomes and J. P. M. Trusler, *J. Chem Thermodyn.* **30**:527 (1998).
15. J. F. Estela-Uribe and J. P. M. Trusler, *Int. J. Thermophys.* **21**:1033 (2000).
16. J. E. Mayer and M. G. Mayer, *Statistical Mechanics* (John Wiley, New York, 1959), p. 469.
17. T. L. Hill, *An Introduction to Statistical Thermodynamics* (Addison–Wesley, Reading, MA, 1960), p. 153.

18. M. W. Chase, C. A. Davies, J. R. Downey, D. J. Frurip, R. A. McDonald, and A. N. Syverud, *J. Phys. Chem. Ref. Data* **14**:1166 (1985).
19. K. A. Gillis and M. R. Moldover, *Int. J. Thermophys.* **17**:1305 (1996).
20. J. P. M. Trusler, W. A. Wakeham, and M. P. Zarari, *Mol. Phys.* **90**:695 (1997).
21. J. J. Hurly, *Int. J. Thermophys.* **21**:805 (2000).
22. J. J. Hurly, D. R. Defibaugh, and M. R. Moldover, *Int. J. Thermophys.***21**:739 (2000).
23. J. J. Hurly, *Int. J. Thermophys.* **21**:185 (2000).
24. T. Kihara, *Rev. Mod. Phys.* **25**:831 (1953).
25. E. A. Mason and T. H. Spurling, *The Virial Equation of State* (Pergamon Press, Oxford, 1969).
26. R. J. Dulla, J. S. Rowlinson, and W. R. Smith, *Mol. Phys.* **21**:229 (1971).
27. R. F. Boisvert, S. E. Howe, D. K. Kahaner, and J. L. Springmann, *The Guide to Available Mathematical Software*, NISTIR 90-4237 (1990).
28. B. M. Axilrod and E. J. Teller, *J. Chem. Phys.* **11**:299 (1943).
29. J. P. M. Trusler, *Int. J. Thermophys.* **18**:635 (1997).
30. A. Eucken and R. Becker, *Z. Phys. Chem.* **B27**:235 (1935).
31. M. W. Chase Jr., *J. Phys. Chem. Ref. Data* **9**:1 (1998).
32. *Selected Values of Properties of Chemical Compounds; Data Project* (Thermodynamics Research Center, Texas A&M University, College Station, 1980–extant), loose-leaf data sheets.
33. D. R. Stull and G. C. Sinke, *Thermodynamic Properties of the Elements* (American Chemical Society, Washington, DC, 1956).
34. T. H. Laby and G. W. C. Kaye, *Tables of Physical and Chemical Constants*, 14th ed. (Longman Group, London, 1973).
35. U. Hohm and U. Trümper, *J. Chem. Soc. Faraday Trans.* **91**:1277 (1995).
36. P. A. Morrison, Ph.D. thesis (California Institute of Technology, Pasadena, 1972) [$B(T)$ values cited by M. Bohn, R. Lustig, and J. Fischer, *Fluid Phase Equil.* **25**:251 (1986)].
37. A. Eucken and G. Hoffmann, *Z. Phys. Chem.* **5B**:4442 (1929).